THE JOURNAL OF PHYSICAL CHEMISTRY B

Article

pubs.acs.org/JPCB

Electron-Attachment-Induced DNA Damage: Instantaneous Strand Breaks

Emilie Cauët,*[,†,‡] Stuart Bogatko,[†] Jacques Liévin,[‡] Frank De Proft,[†] and Paul Geerlings[†]

[†]General Chemistry - Algemene Chemie, Vrije Universiteit Brussel, Pleinlaan 2, B-1050 Brussels, Belgium

[‡]Service de Chimie Quantique et Photophysique, Université Libre de Bruxelles, Avenue F.D. Roosevelt 50, CPi160/09, B-1050 Brussels, Belgium

Supporting Information

ABSTRACT: Low energy electron-attachment-induced damage in DNA, where dissociation channels may involve multiple bonds including complex bond rearrangements and significant nuclear motions, is analyzed here. Quantum mechanics/molecular mechanics (QM/MM) calculations reveal how rearrangements of electron density after vertical electron attachment modulate the position and dynamics of the atomic nuclei in DNA. The nuclear motions involve the elongation of the P−O (P−$O_{3'}$ and P−$O_{5'}$) and C−C ($C_{3'}$−$C_{4'}$ and $C_{4'}$−$C_{5'}$) bonds for which the acquired kinetic energy becomes high enough so that the neighboring $C_{3'}$−$O_{3'}$ or $C_{5'}$−$O_{5'}$ phosphodiester bond may break almost immediately. Such dynamic behavior should happen on a very short time scale, within 15−30 fs, which is of the same order of magnitude as the time scale predicted for the excess electron to localize around the nucleobases. This result indicates that the C−O phosphodiester bonds can break before electron transfer from the backbone to the base.

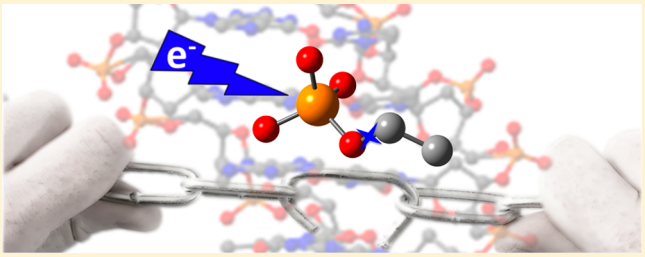

INTRODUCTION

Low energy electrons (LEEs), produced in large quantity along all of the tracks of ionizing radiation, are known to cause DNA damage and mutations. In particular, LEEs can act directly on DNA to induce single strand breaks (SSBs) and double strand breaks (DSBs).[1−5] These effects have stimulated a need to elucidate the direct strand break mechanisms most likely involved. Studies showed that electrons with energies below 30 eV can attach to DNA components, forming transient anion states of DNA subunits (a base, sugar, or phosphate group). In this manner, LEEs induce SSBs and DSBs principally via the decay of transient anion states into dissociating electronically excited states and dissociative electron attachment (DEA).[5−7] However, which bonds break in the SSBs and DSBs and the details of the motions of the nuclei during the lifetime of the dissociating states were not resolved yet.

While studies have led to a picture of strand breaks (SBs) likely involving the $C_{3'}$−$O_{3'}$ or $C_{5'}$−$O_{5'}$ phosphodiester bonds breaking along the DNA backbone (Figure 1), the precise mechanism of this process continues to be debated. It is not clear that this occurs due to the initial formation of a backbone-centered radical anion[8] (the LEE is captured first by a sugar−phosphate group) or by the initial formation of a base-centered radical anion[9−12] (the LEE first attaches to the π^* orbitals of nucleobases) in which the subsequent SBs are promoted by an excess electron transfer from the base to the sugar−phosphate backbone. In both cases, computation of energy profiles shows that barriers for $C_{3'}$−$O_{3'}$ or $C_{5'}$−$O_{5'}$ bond cleavage are small (∼7−15 kcal/mol in the gas phase and ∼14−25 kcal/mol in an aqueous solution).[8,10,13−15] Smyth and Kohanoff performed dynamical simulations of an excess electron in condensed phase models of solvated DNA bases after vertical attachment, indicating that the excess electron, which is initially found to be delocalized, gets localized around the nucleobases within a 15−25 fs time scale.[16] Recently, the same authors showed that thermal fluctuations of the solvent around DNA bases induce energy barriers for $C_{3'}$−$O_{3'}$ bond cleavage as low as ∼6 kcal/mol (except for dAMP; 10 kcal/mol).[17]

Although the rupture of the N-glycosidic $C_{1'}$−N bond between the sugar and the base has also been considered (Figure 1), it has rapidly been discarded on the basis of the high-energy barrier estimated for this reaction (∼19−22 kcal/mol in the gas phase and ∼20−29 kcal/mol in an aqueous solution, both based on the base-centered radical anion mechanism).[15,18−20] Experimentally, Li et al. speculated that the N-glycosidic bond cleavage is suppressed in long DNA polymers because this cleavage has been observed exclusively from the termini of short model oligonucleotides.[21,22] Other possible routes are the breakage of the P−$O_{3'}$ and P−$O_{5'}$ or even the $C_{4'}$−$C_{5'}$ bonds (Figure 1) which would result in immediate DNA SBs. Radicals associated with cleavage of P−O bonds have been reported in electron spin resonance

Received: June 26, 2013
Revised: July 12, 2013
Published: July 19, 2013

 © 2013 American Chemical Society dx.doi.org/10.1021/jp406320g | J. Phys. Chem. B 2013, 117, 9669−9676

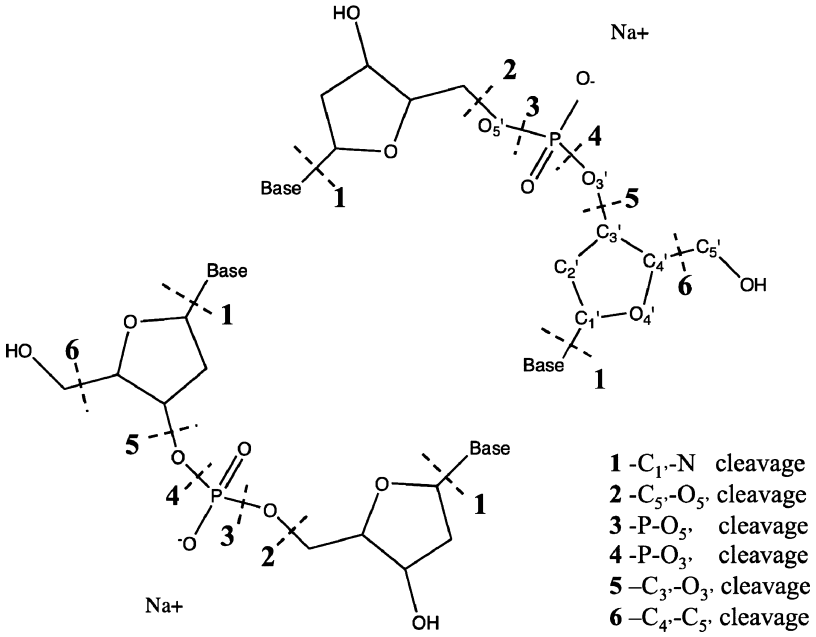

Figure 1. Structure of the 5′-d*X*pd*Y*-3′ two-base-pair duplex (where *X* and *Y* are one of the four nucleobases T, C, A, and G) and positions of cleavage for the N-glycosidic bond (1) and C−O (2−5), P−O (3−4), and C−C (6) bonds.

experiments on DNA irradiated at low temperatures.[23,24] Sanche's and Simons' studies suggest, however, that the P−O bond cleavage is minor compared to the C−O bond cleavage.[25−27] Rak and co-workers tackled the possibility of P−O bond dissociation by proposing a mechanism of SSB in DNA that starts with the LEE attachment to the nucleotide of thymine followed by the protonation of the base.[28]

In the mechanistic models discussed above, the energetics of different fragmentation routes involving particular bonds have been tested while the corresponding bonds have been supposed to stretch enough (either before or after electron attachment) to reach the barrier of the fragmentation reaction on the energy profile of the anion. However, in large polyatomic molecules such as DNA, dissociation channels may involve multiple bonds including complex bond rearrangements and significant nuclear motions. Moreover, the presence of water around DNA, which was demonstrated to modify the dissociation channels and thus the SSB and DSB yield functions,[16,17,29] limits the validity and applicability of treatments that do not explicitly incorporate it. In order to obtain a complete picture of DNA damage induced by LEE, an essential question thus remains to be answered: What are the most important rearrangements in the nuclear geometry of the DNA components, within a realistic environment, due to the initial electron attachment?

We report results obtained by first-principles density functional theory (DFT) calculations of native and reduced (by vertical attachment of one electron) configurations of 2-base pair (bp) B-DNA duplexes (dTpdT, dCpdC, and dTpdC where p represents the phosphate group) with an intact sugar−phosphate backbone and including the neutralizing Na^+ counterions (Figure 1). The oligomers were chosen because they are composed of the easiest DNA bases to reduce (e.g., T and C).[30] Configurations were selected from independent room temperature classical molecular dynamics (MD) simulations of 12-bp duplexes (Figure 2). DFT calculations were based on a combined quantum mechanics/molecular mechanics (QM/MM) model in which a large (and more realistic) representation of the environment surrounding the 2-bp B-DNA duplex was included that involves the rest of the DNA fragment, counterions, and an explicit representation of the water solvent molecules.

Concepts based on conceptual DFT (CDFT),[31] in which our group has been very active,[32,33] were used to investigate the coupling of the electronic perturbation, induced by attachment of an electron, to the initial structural reorganization leading to SBs. We focused on the evaluation of two CDFT reactivity descriptors: the electronic and nuclear Fukui functions. The electronic Fukui function[34] ($f^+(r)$) represents the response of the electron density to electron attachment, while the nuclear Fukui function[35] (Φ_α^+) characterizes the forces that the atomic nuclei experience due to electron attachment and captures the onset of the change in the nuclear positions induced by a change in the number of electrons. Whereas the electronic Fukui function gained widespread use,[32,33] its nuclear part has been less addressed[36,37] and their combined use was exploited only in a few studies mainly concentrating on Jahn−Teller distortion[38,39] for small molecules. Here we show that that these concepts are true and trustworthy companions to gain insight into the way electron-attachment-induced structural perturbations may be influencing the formation of SSBs and DSBs in DNA.

■ COMPUTATIONAL DETAILS

Three 12-mer fragments of B-DNA were considered in this study:

(1) 3′-TTTTTTTTTTTT-5′
(2) 3′-CCCCCCCCCCCC-5′
(3) 3′-AGCGCTATGCGA-5′

The underlined letters indicate the 2-bp DNA in the QM region of the subsequent QM/MM calculations. All fragments were created as a linear chain of nucleotides, using idealized B-DNA geometries, with the Biosym Insight II software.[40] The solvation, minimization, and equilibration steps and QM/MM calculations were performed with the NWChem program package.[41]

dx.doi.org/10.1021/jp406320g | J. Phys. Chem. B 2013, 117, 9669−9676

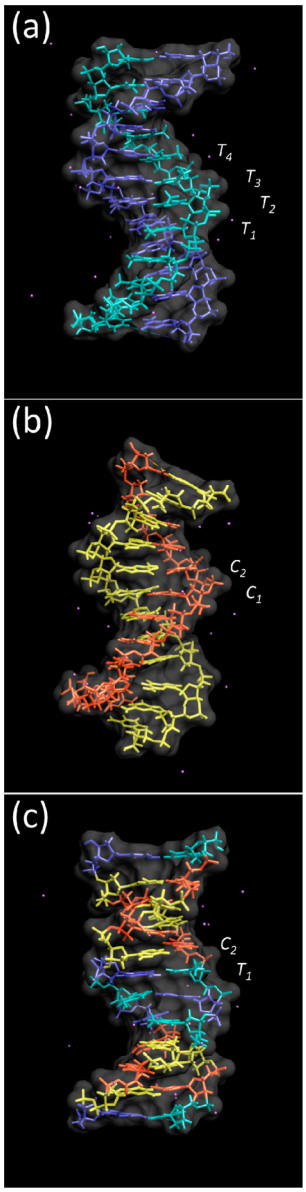

Figure 2. Results from room-temperature classical molecular dynamics simulations of the 12-bp B-DNA duplexes: (a) d(3′-TTTTTTTTTTTT-5′); (b) d(3′-CCCCCCCCCCCC-5′); (c) d(3′-AGCGCTATGCGA-5′). The quantum-mechanical calculations discussed in the text were performed for the 2-bp segments d(5′-T_1pT_2-3′), d(5′-T_3pT_4-3′), d(5′-C_1pC_2-3′), and d(5′-T_1pC_2-3′). The deoxyribonucleosides are distinguished by color as follows: thymine, cyan; cytosine, orange; adenine, blue; guanine, yellow. The Na^+ counterions are represented by purple spheres. The solvating water molecules are not shown.

The DNA fragments 1, 2, and 3 were embedded in a periodic box (51 × 51 × 69 $Å^3$) filled with 5733, 5722, and 5730 water molecules, respectively, at a density of 1.0 g/cm^3. Twenty-two sodium counterions were added to counterbalance the total charge of each fragment. After short steepest descent minimization runs of 1000 steps, an equilibration phase via classical MD was carried out using the AMBER force field[42] for DNA and the sodium counterions and the SPC/E model[43] for the water solvent. The short-range van der Waals interactions were truncated at 15 Å, and the Coulombic interactions were calculated with the particle mesh Ewald method[44,45] (also with a cutoff of 15 Å). All atoms were free to move, and a time step of 1 fs was used. After heating each system from 50 to 298.15 K at constant volume over 60 ps, a production MD (100 ps) was run in the NPT ensemble with the temperature and pressure held constant at 298.15 K and 1 bar, respectively. The resulting equilibrated structures (files jp406320g_si_002.pdb, jp406320g_si_003.pdb, and jp406320g_si_004.pdb provided in the Supporting Information) were used as the QM/MM starting coordinates of the 2-bp duplexes (fragment 1 for dT_1pdT_2 and dT_3pdT_4, 2 for dC_1pdC_2, and 3 for dC_1pdT_2). The QM regions include the DNA bases, the associated sugar groups, the phosphate group bounded to the two sugars, and the respective sodium ions. The valences of the truncated bonds were completed by the addition of hydrogen link atoms. The QM region was described using DFT at the M06-2X[46,47]/6-31+G(d,p) level. The MM region was treated with the AMBER force field and the SPC/E model as implemented in NWChem. The electrostatic interactions between the QM and MM regions were treated with the electrostatic embedding method (inclusion of the MM point charges into the QM Hamiltonian).

Two separate QM/MM calculations, performed on the neutral and anionic species, were carried out for each 2-bp duplex. The restricted and unrestricted M06-2X formalism was employed for the neutral and anion species, respectively. VEAs were computed as the difference between the absolute energies of the neutral and anion species at the neutral structure:

$$\mathrm{VEA} = E_{\mathrm{neutral}} - E_{\mathrm{anion}} \tag{1}$$

The electronic Fukui function, $f(r)$, already presented in the Introduction, characterizes changes of the electron density $\rho(r)$, at each point r, when the total number of electrons (N) is changed:

$$f(r) = \left(\frac{\partial \rho(r)}{\partial N}\right)_{\nu} \tag{2}$$

The nuclear Fukui function, Φ_α, characterizes the changes in the force (F) that the nucleus α experiences when the total number of electrons (N) of the system is changed:

$$\Phi_\alpha = \left(\frac{\partial F_\alpha}{\partial N}\right)_{\nu} \tag{3}$$

In both eqs 2 and 3, $\nu(r)$ is the external potential defined by nuclear charges and positions.

When evaluating $f(r)$ and Φ_α, one is confronted with the differentiation with respect to N, which for an isolated molecule is necessarily an integral number, and the discontinuity of the derivative. To circumvent this problem, Fukui function calculations use the finite difference method, approximating $f(r)$ and Φ_α for a reaction provoking an electron increase in the system as

$$f^+(r) = \rho_{N+1}(r) - \rho_N(r) \tag{4}$$

where ρ_{N+1} and ρ_N represent the electron density function of the anionic and neutral species, respectively, and

$$\Phi_\alpha^+ = F_\alpha(N+1) - F_\alpha(N) \tag{5}$$

where $F_\alpha(N+1)$ and $F_\alpha(N)$ are the forces (energy gradients) acting on nuclei of the anionic and neutral species, respectively.

Note that, in view of the nature of the Fukui functions (the demand for a fixed external potential in 2 and 3, so fixed

dx.doi.org/10.1021/jp406320g | J. Phys. Chem. B 2013, 117, 9669−9676

nuclei), the electron density function and forces on the anion species were calculated with the same geometry as the neutral system. Thus, the applicability of the Fukui functions for understanding the electron-attachment-induced structural perturbations follows the assumption that changes in the electron density lead to the reorganization of the nuclear geometry (electron preceding picture).[48]

Using physical laws forming the basis of classical mechanics, we performed an estimate of the amount of kinetic energy (KE) delivered to bonds in the 2-bp B-DNA duplexes. KE was estimated as a sum of the KE_α delivered to each nucleus involved in the bond:

$$KE_\alpha = \frac{1}{2} m_\alpha (v_\alpha)^2 \tag{6}$$

where m and v are the nuclear mass and velocity, respectively. Making the simplifying assumption that the nucleus' initial velocity is zero, its v, after a period of time Δt, is

$$v_\alpha = a_\alpha \Delta t \tag{7}$$

where a is the nuclear acceleration, supposed here to be constant. As described by Newton's second law, the nucleus' acceleration is parallel and directly proportional to the nucleus force Φ_α^+ (projected here along the bond) and inversely proportional to its mass m.

RESULTS

Results obtained from the DFT QM/MM simulations for the 2-bp duplexes dT_1pdT_2, dT_3pdT_4, dC_1pdC_2, and dT_1pdC_2 are shown in Figures 3 and 4. These 2-bp duplexes are all very good electron acceptors. The vertical electron affinities (VEAs) of dT_1pdT_2, dT_3pdT_4, dC_1pdC_2, and dT_1pdC_2 calculated in the presence of a fully solvated DNA environment are 7.17, 7.19, 7.34, and 7.40 eV, respectively. Energetically, the electron-capturing behavior of each 2-bp duplex is predicted to be the same (less than 0.2 eV of difference). The large VEA values of the 2-bp duplexes originate from increased stability of the radical anion caused by the solvating water molecules.[5,49]

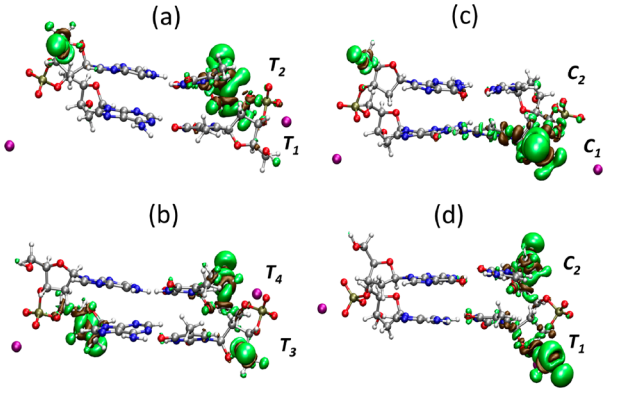

Figure 3. Electronic Fukui function $f^+(\mathbf{r})$ of (a) d(5′-T_1pT_2-3′), (b) d(5′-T_3pT_4-3′), (c) d(5′-C_1pC_2-3′), and (d) d(5′-T_1pC_2-3′) 2-bp duplexes (M062X/6-31+G(d,p)). Green isodensity surface, +0.0015 atomic units; ochre surface, −0.0015 atomic units. The electronic Fukui function $f^+(\mathbf{r})$ function describes how the electron density of each 2-bp duplex changes in the crucial step of electron attachment. The ochre isosurface (negative value of the electronic Fukui function) encloses the region that loses electron density during charge transfer, while the green isosurface (positive value of the electronic Fukui function) encloses the region that gains electron density when the system is overall gaining one electron.

The electronic Fukui functions of dT_1pdT_2, dT_3pdT_4, dC_1pdC_2, and dT_1pdC_2 are depicted in Figure 3a−d. These figures show how the electron density of each 2-bp duplex changes in the crucial step of electron attachment. The ochre isosurface (negative value of the electronic Fukui function) encloses the region that loses electron density during charge transfer, while the green isosurface (positive value of the electronic Fukui function) encloses the region that gains electron density when the system is overall gaining one electron. Globally, the electron density changes induced by the electron attachment on the 2-bp duplexes appear on the pyrimidine deoxyribonucleosides dT and dC. This result is consistent with the relative sensitivity of deoxyribonucleosides to LEEs and correlates with their electron affinity, as determined experimentally and as supported by theoretical calculations.[50,51] Furthermore, the electron density changes are more prominent on the sugar unit of the deoxyribonucleosides than on the base. Large positive values of the electronic Fukui function show up in all the bond regions with the sugar ring carbon atoms. These positive values correspond to an accumulation of the electron density, which is expected to favor an increase of the sugar bond lengths. No major electronic Fukui functions are obtained on the phosphate group between deoxyribonucleosides. Some positive electron Fukui values occur, however, on the phosphate group between the two dTs in dT_1pdT_2 and between the two dCs in dC_1pdC_2. In the dT_3pdT_4 2-bp duplex, some electron density rearrangements also appear on the sugar unit of the deoxyadenosine 3′-dA. Furthermore, highly local electron density changes appear around the oxygen $O_{5'}$ of 5′-dA in dT_1pdT_2, of 5′-dT (dT_3) in dT_3pdT_4, and of 5′-dG in dC_1pdC_2. Overall, we note that the electron Fukui function values on the oxygen atoms (either $O_{5'}$ or $O_{3'}$) at the termini of our model tend to increase. This effect may be interpreted as boundary artifacts due to the difference in effective chemical potential between the QM and MM regions, which leads to an artificial excess polarization, and concomitant density inhomogeneity nearer to the QM/MM boundary.[52,53] The excess polarization on the $O_{5'}$ and $O_{3'}$ oxygen atoms at the termini of our model is suggested as a possible source of errors in the calculations of the forces experienced by these atoms (that are actually found to be very large). For this reason, only the forces on the $O_{5'}$ and $O_{3'}$ atoms distant from the QM/MM boundary are discussed below.

The nuclear Fukui function magnitudes ($|\Phi_\alpha^+|$) for each atomic site in the dT_1pdT_2, dT_3pdT_4, dC_1pdC_2, and dT_1pdC_2 2-bp duplexes are given in Tables S1−S4 of the Supporting Information. However, because the direction of the forces also influences their effects on the bonds in 2-bp duplexes, we projected the atomic forces in the direction of all the bonds formed by the atom. The vector representations of the projected nuclear Fukui functions for the heavy atoms in dT_1pdT_2, dT_3pdT_4, dC_1pdC_2, and dT_1pdC_2 are depicted in Figure 4a−d. Only the forces corresponding to bond elongations are represented with the goal of identifying all possible bond dissociation reactions. Vector lengths (small to large) reflect relative magnitudes of the projected nuclear Fukui functions within each 2-bp duplex (only magnitudes larger than 0.5 nN are noted). Generally, the similarity between Figures 3 and 4 underlines the interplay between electron density rearrangements and nuclear displacements in the important

dx.doi.org/10.1021/jp406320g | J. Phys. Chem. B 2013, 117, 9669−9676

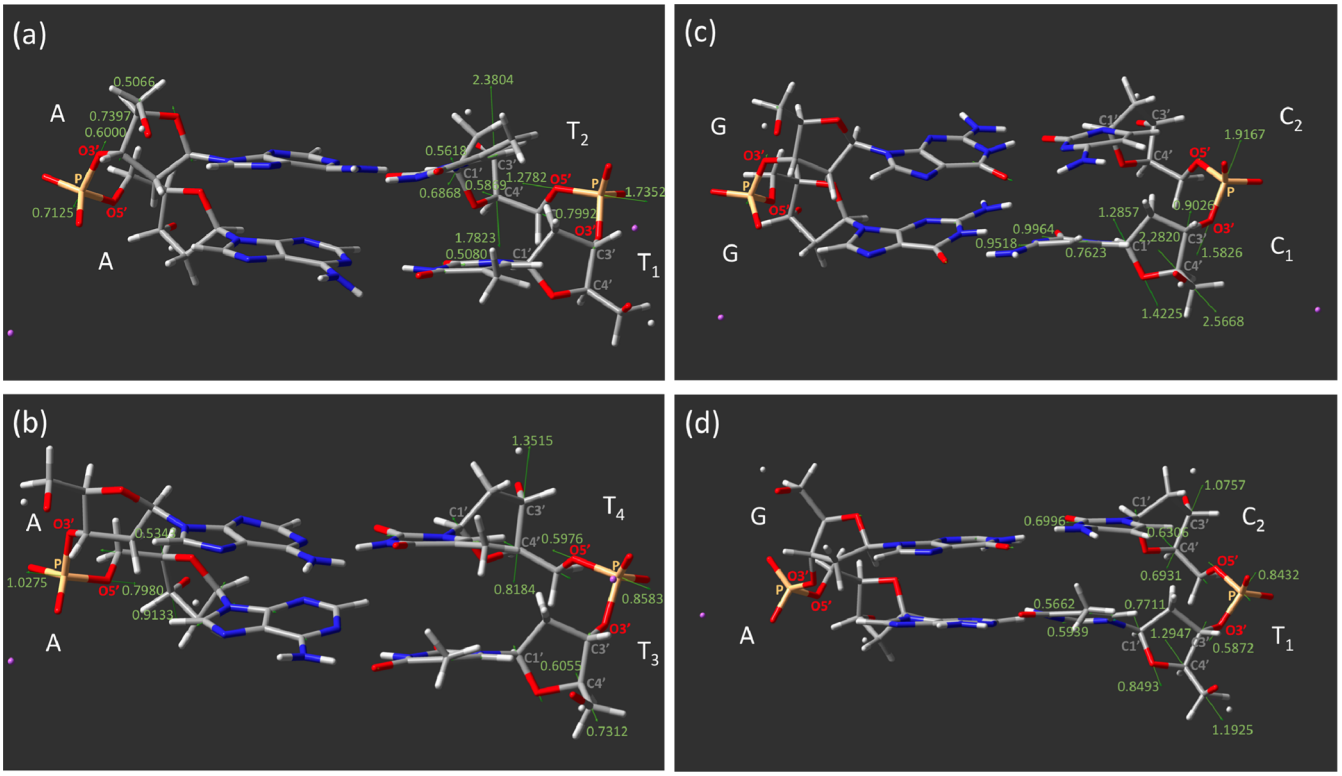

Figure 4. Vector representations of the projected nuclear Fukui functions (Φ_α^+) for the heavy atoms in (a) d(5′-T_1pT_2-3′), (b) d(5′-T_3pT_4-3′), (c) d(5′-C_1pC_2-3′), and (d) d(5′-T_1pC_2-3′) 2-bp duplexes (M062X/6-31+G(d,p)). Only the forces corresponding to bond elongations are represented with the goal of identifying all possible bond dissociation reactions. Vector lengths (small to large) represent relative magnitudes of the nuclear Fukui functions within each 2-bp duplex (magnitudes larger than 0.5 nN are noted).

step of electron attachment on the 2-bp duplexes; i.e., important electron density changes tend to induce large dissociative nuclear forces. Thus, as the most important electron density changes induced by the electron attachment occur on the pyrimidine deoxyribonucleosides, the sums of $|\Phi_\alpha^+|$ for each atom are larger for the dT and dC pyrimidine compared to the dA and dG purine deoxyribonucleosides.

The nuclear Fukui function data help us to interpret several trends as they pertain to the initial mechanistic steps of electron-induced DNA damage proposed in the literature. For each 2 bp-duplex, nuclear Fukui function data seem to indicate that the cleavage of the N-glycosidic bond between a base and its deoxyribose (Figure 1) is not a likely initial mechanistic step for dissociation. Indeed, if the breakage of the N-glycosidic bond resulting in base release was very likely, the largest nuclear Fukui function responses would occur for a bonded $C_{1'}$–N_1 pair in dT and dC or for a bonded $C_{1'}$–N_9 pair in dA and dG. However, there is no evidence of a significantly large force response on any atoms of these pairs in any 2-bp duplex. Even though $C_{1'}$ has a larger magnitude of response in dT_2 of dT_1pdT_2 (1.25 nN), in dC_1 of dC_1pdC_2 (1.39 nN), and in dT_1 of dT_1pdC_2 (0.94 nN) than in the other deoxyribonucleoside, the force response occurs essentially between the bonded atoms $C_{1'}$–$O_{4'}$ and not between $C_{1'}$–N_1. This is clearly illustrated in Figure 4, which shows roughly 0 nN forces on the $C_{1'}$–N bonds, providing evidence that cleavage of the N-glycosidic bond does not appear to be a likely pathway for electron attached dTpdT, dCpdC, and dTpdC 2-bp duplexes. This is consistent with the predictions previously reported in the literature.[21,22]

Nuclear Fukui function data indicate that reactivity of the dTpdT, dCpdC, and dTpdC 2-bp duplexes due to the addition of an electron will tend to involve the breakage of the phosphodiester bonds more than the N-glycosidic bonds. This is evidenced, for each 2-bp duplex, by large projected force responses between the sugar–phosphate backbone atoms (Figure 4). Moreover, projected force responses in Figure 4a and b show that reactivity as a result of adding an electron to the dTpdT 2-bp duplex may affect both strands of the duplex (i.e., DSB), while, in dCpdC and dTpdC, only the strand on which the pyrimidine bases are located is likely to be altered (i.e., SSB). For both strands of the dTpdT 2-bp duplex (either dT_1pdT_2 or dT_3pdT_4), projected force responses indicate that the elongation of a P–O bond is a likely initial mechanistic step for fragmentation (combined magnitude of projected forces up to 3.01 nN). Although the elongation of the P–$O_{5'}$ bond seems favored, the P–$O_{3'}$ extension appears a possible reaction as well (combined magnitude of 1.31 nN for P–$O_{3'}$ between the two adjacent adenine bases in dT_1pdT_2). In both dC_1pdC_2 and dT_1pdC_2 2-bp duplexes, elongation of a P–O bond between the two pyrimidine bases may also occur. The P–O elongation seems here favored between the phosphate atom and the 3′ oxygen atom. The combined magnitude of the projected forces along the P–$O_{3'}$ bond is 3.50 and 1.43 nN in dC_1pdC_2 and dT_1pdC_2, respectively. We note that very small values are found for their counterpart in the opposite strand (0.80 and 0.28 nN in dC_1pdC_2 and dT_1pdC_2, respectively). Electron attachment to the dTpdT, dCpdC, and dTpdC 2-bp duplexes also requires the elongation of the $C_{5'}$–$C_{4'}$ bonds. This event appears to be plausible given the nuclear Fukui function magnitudes and directions for the $C_{5'}$ and $C_{4'}$ atoms in both nucleoside dT and

dx.doi.org/10.1021/jp406320g | J. Phys. Chem. B 2013, 117, 9669–9676

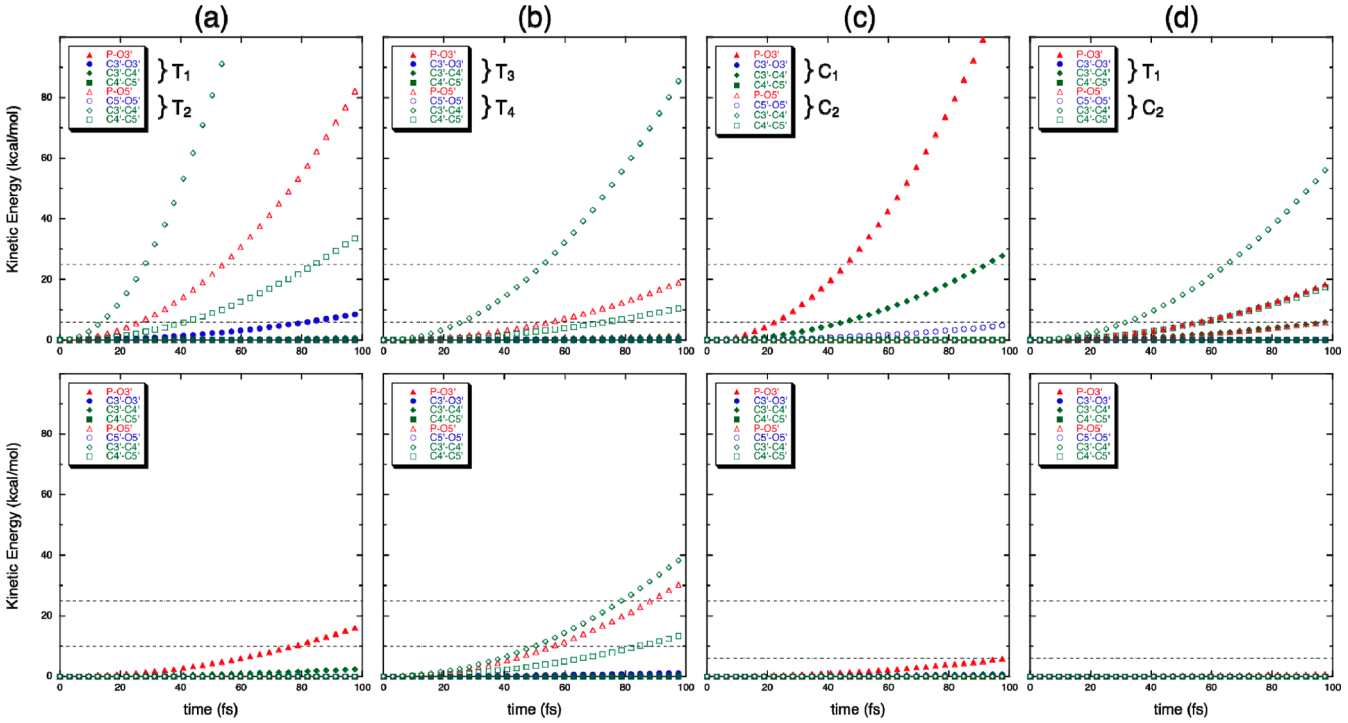

Figure 5. Estimated amount of kinetic energy (KE) (in kcal/mol) delivered, as a function of time, to the selected P−O (P−$O_{3'}$ and P−$O_{5'}$, triangles), C−O ($C_{3'}$−$O_{3'}$ and $C_{5'}$−$O_{5'}$, circles), C−C ($C_{3'}$−$C_{4'}$, diamonds; $C_{4'}$−$C_{5'}$, squares) bonds in the (a) dT_1pdT_2, (b) dT_3pdT_4, (c) dC_1pdC_2, and (d) dT_1pdC_2 2-bp duplexes once the electron has attached. The upper part of each panel corresponds to the bonds of the strand on which the pyrimidine bases are located, and the lower part corresponds to their counterpart in the opposite strand. For some bonds, KE raises very rapidly to values corresponding to the estimated range (6−25 kcal/mol except for dAs 10−25 kcal/mol; dotted horizontal lines) of energy barriers leading to SBs. The data is plotted on a 100 fs time scale corresponding to the C−O vibrational rate (10^{13} s^{-1}).

dC of each 2-bp duplex. The combined magnitudes for $C_{5'}$−$C_{4'}$ reach values of 1.39, 1.34, 4.85, and 2.49 nN in dT_1pdT_2, dT_3pdT_4, dC_1pdC_2, and dT_1pdC_2 2-bp duplexes, respectively. The elongation of the $C_{3'}$−$C_{4'}$ bond seems possible as well given the appreciable force responses on these sugar atoms (combined magnitudes up to 4.16, 2.17, 0.90, and 1.77 nN in dT_1pdT_2, dT_3pdT_4, dC_1pdC_2, and dT_1pdC_2 2-bp duplexes, respectively).

We performed an estimate of the amount of KE delivered, as a function of time, to the P−O (P−$O_{3'}$ and P−$O_{5'}$), C−O ($C_{3'}$−$O_{3'}$ and $C_{5'}$−$O_{5'}$), and C−C ($C_{3'}$−$C_{4'}$ and $C_{4'}$−$C_{5'}$) bonds in the dT_1pdT_2, dT_3pdT_4, dC_1pdC_2, and dT_1pdC_2 2 bp-duplexes (Figure 5a−d) once the electron has attached. Upper parts of each panel correspond to the bonds of the strand on which the pyrimidine bases are located, and lower parts correspond to their counterpart in the opposite strand. The initial effects would likely occur on the strand with pyrimidine bases for which the KE of the bonds rises much more rapidly. For this strand, bonds such as P−$O_{3'}$, P−$O_{5'}$, $C_{3'}$−$C_{4'}$, and $C_{4'}$−$C_{5'}$ exhibit KE in the range 6−25 kcal/mol after only ∼15−30 fs (much less than the vibrational time scale of C−O ∼100 fs). These energies are of the same order of magnitude as the energy barriers (dotted horizontal lines) estimated for a $C_{3'}$−$O_{3'}$ or $C_{5'}$−$O_{5'}$ bond breaking in an aqueous solution. Indeed, Leszczynski's group[13−15] revealed that the $C_{3'}$−$O_{3'}$ and $C_{5'}$−$O_{5'}$ bonds can break after surmounting an energy barrier of ∼14 and 18−22 kcal/mol, respectively, in an aqueous solution, while Simons and co-workers[10] predicted a higher energy barrier for $C_{3'}$−$O_{3'}$ bond cleavage (∼25 kcal/mol in an aqueous solution). Smyth and Kohanoff predicted that thermal fluctuations of the solvent induce energy barriers for $C_{3'}$−$O_{3'}$ bond cleavage as low as ∼6 kcal/mol (except for dAMP; 10 kcal/mol).[17] Thus, although the breakage of the P−O (P−$O_{3'}$ or P−$O_{5'}$) and nonpolar C−C ($C_{3'}$−$C_{4'}$ or $C_{4'}$−$C_{5'}$) bonds are less likely to occur as initial steps in the electron-attachment-induced DNA SBs, the effects of the dynamics of these bonds upon displacement of the $O_{3'}$, $O_{5'}$, $C_{3'}$, and $C_{5'}$ atoms may be significant. This can be viewed as a simple system of three coupled oscillators in which the energy transfers from one oscillator to the other. The energies of the P−$O_{3'}$ and $C_{3'}$−$C_{4'}$ bonds may thus be transferred to the $C_{3'}$−$O_{3'}$ bond, while the energies of the P−$O_{5'}$ and $C_{4'}$−$C_{5'}$ bonds may be transferred to the $C_{5'}$−$O_{5'}$ bond. According to the KE distributions, the effects of the dynamic behaviors of the P−O and C−C bonds may thus be significant, enabling immediate C−O (either $C_{3'}$−$O_{3'}$ or $C_{5'}$−$O_{5'}$) bond cleavage.

CONCLUSION

From our studies, we conclude that before thermalization the vertical attachment of an electron on a 2-bp B-DNA duplex occurs on the sugar−phosphate backbone. Moreover, the forces on the atomic nuclei, which govern the changes in their position in response to change in the electron number, become already significant at the instant of electron attachment. Of particular importance are large elongation forces on backbone sites, which weaken mainly the P−O (P−$O_{3'}$ and P−$O_{5'}$) and C−C ($C_{3'}$−$C_{4'}$ and $C_{4'}$−$C_{5'}$) bonds. The supplied KE to these bonds is found to be in excess of any previously estimated energy barriers leading to SBs.

dx.doi.org/10.1021/jp406320g | J. Phys. Chem. B 2013, 117, 9669−9676

From these findings, a microscopic mechanism of LEE-induced SBs in DNA emerges that is governed, at the nascent stage, by the electron density perturbations and the resulting initial spatial motions of the nuclei required to accommodate the excess electron. As we said, the nuclear motions involve the elongation of the P−O (P−$O_{3'}$ and P−$O_{5'}$) and C−C ($C_{3'}$−$C_{4'}$ and $C_{4'}$−$C_{5'}$) bonds for which the exhibited KE becomes high enough so that the neighboring $C_{3'}$−$O_{3'}$ or $C_{5'}$−$O_{5'}$ phosphodiester bond may break. We show that this should happen in very short times, within a 15−30 fs time scale. This time scale is of the same order of magnitude as the time scale predicted for the excess electron to localize around the nucleobases (∼15−25 fs),[16] indicating that the C−O bonds may break almost instantaneously, before electron transfer from the sugar−phosphate backbone to the base. It is worth noticing that all these chemical reactions leading to SBs will have to compete with the fast electron autodetachment process (∼10 fs).[10] The reactions leading to SBs will also be in competition with protonation of the nucleotides by water. However, even if protonation is faster than bond cleavage, this does not change the relevance of our current findings because protonation of the nucleotides is not expected to affect the bond cleavage energetics.[54]

■ ASSOCIATED CONTENT

Supporting Information

Equilibrated structures used as the QM/MM starting coordinates of the 2-bp duplexes (fragment 1 for dT_1pdT_2 and dT_3pdT_4, fragment 2 for dC_1pdC_2, and fragment 3 for dC_1pdT_2). Tables with the nuclear Fukui function magnitudes ($|\Phi_\alpha^+|$) (in nN) for each atomic site in the dT_1pdT_2, dT_3pdT_4, dC_1pdC_2, and dT_1pdC_2 2-bp duplexes. This material is available free of charge via the Internet at http://pubs.acs.org.

■ AUTHOR INFORMATION

Corresponding Author

*E-mail: ecauet@ulb.ac.be. Phone: +32 2 650 2057.

Author Contributions

The manuscript was written through contributions of all authors. All authors have given approval to the final version of the manuscript.

Notes

The authors declare no competing financial interest.

■ ACKNOWLEDGMENTS

E.C. thanks the Francqui Foundation for providing a Scientific Mandate of Intercommunity Scientific Postdoctoral Collaborator. S.B. thanks the Vrije Universiteit Brussel (VUB) for providing a postdoctoral position. P.G. and F.D.P. thank the VUB and the FWO-Flanders for continuous support to their lab. E.C. and J.L. thank the Communauté française of Belgium (Action de Recherche Concertée) for financial support.

■ REFERENCES

(1) Boudaïffa, B.; Cloutier, P.; Hunting, D.; Huels, M. A.; Sanche, L. Resonant Formation of DNA Strand Breaks by Low-Energy (3 to 20 eV) Electrons. *Science* **2000**, *287*, 1658−1660.

(2) Martin, F.; Burrow, P. D.; Cai, Z.; Cloutier, P.; Hunting, D.; Sanche, L. DNA Strand Breaks Induced by 0−4 eV Electrons: The Role of Shape Resonances. *Phys. Rev. Lett.* **2004**, *93*, 068101.

(3) Baccarelli, I.; Bald, I.; Gianturco, F. A.; Illenberger, E.; Kopyra, J. Electron-Induced Damage of DNA and Its Components: Experiments and Theoretical Models. *Phys. Rep.* **2011**, *508*, 1−44.

(4) Keller, A.; Bald, I.; Rotaru, A.; Cauët, E.; Gothelf, K. V.; Besenbacher, F. Probing Electron-Induced Bond Cleavage at the Single-Molecule Level Using DNA Origami Templates. *ACS Nano* **2012**, *6*, 4392−4399.

(5) Alizadeh, E.; Sanche, L. Precursors of Solvated Electrons in Radiobiological Physics and Chemistry. *Chem. Rev.* **2012**, *112*, 5578−5602.

(6) Huels, M. A.; Boudaïffa, B.; Cloutier, P.; Hunting, D.; Sanche, L. Single, Double, and Multiple Double Strand Breaks Induced in DNA by 3−100 eV Electrons. *J. Am. Chem. Soc.* **2003**, *125*, 4467−4477.

(7) Sanche, L. *Radical and Radical Ion Reactivity in Nucleic Acid Chemistry*; John Wiley and Sons: Hoboken, NJ, 2009.

(8) Li, X.; Sevilla, M. D.; Sanche, L. Density Functional Theory Studies of Electron Interaction with DNA: Can Zero eV Electrons Induce Strand Breaks? *J. Am. Chem. Soc.* **2003**, *125*, 13668−13669.

(9) Barrios, R.; Skurski, P.; Simons, J. Mechanism for Damage to DNA by Low-Energy Electrons. *J. Phys. Chem. B* **2002**, *106*, 7991−7994.

(10) Simons, J. How Do Low-Energy (0.1−2 eV) Electrons Cause DNA-Strand Breaks? *Acc. Chem. Res.* **2006**, *39*, 772−779.

(11) Zheng, Y.; Wagner, J. R.; Sanche, L. DNA Damage Induced by Low-Energy Electrons: Electron Transfer and Diffraction. *Phys. Rev. Lett.* **2006**, *96*, 208101.

(12) Gu, J.; Leszczynski, J.; Schaefer, H. F. Interactions of Electrons with Bare and Hydrated Biomolecules: From Nucleic Acid Bases to DNA Segments. *Chem. Rev.* **2012**, *112*, 5603−5640 (and references therein).

(13) Gu, J.; Wang, J.; Leszczynski, J. Electron Attachment-Induced DNA Single Strand Breaks: C3′-O3′ σ-Bond Breaking of Pyrimidine Nucleotides Predominates. *J. Am. Chem. Soc.* **2006**, *128*, 9322−9323.

(14) Bao, X.; Wang, J.; Gu, J.; Leszczynski, J. DNA Strand Breaks Induced by Near-Zero-Electronvolt Electron Attachment to Pyrimidine Nucleotides. *Proc. Natl. Acad. Sci. U.S.A.* **2006**, *103*, 5658−5663.

(15) Gu, J.; Wang, J.; Leszczynski, J. Low Energy Electron Attachment to the Adenosine Site of DNA. *J. Phys. Chem. B* **2011**, *115*, 14831−14837.

(16) Smyth, M.; Kohanoff, J. Excess Electron Localization in Solvated DNA Bases. *Phys. Rev. Lett.* **2011**, *106*, 238108.

(17) Smyth, M.; Kohanoff, J. Excess Electron Interactions with Solvated DNA Nucleotides: Strand Breaks Possible at Room Temperature. *J. Am. Chem. Soc.* **2012**, *134*, 9122−9125.

(18) Gu, J.; Xie, Y.; Schaefer, H. F. Glycosidic Bond Cleavage of Pyrimidine Nucleosides by Low-Energy Electrons: A Theoretical Rationale. *J. Am. Chem. Soc.* **2005**, *127*, 1053−1057.

(19) Li, X.; Sanche, L.; Sevilla, M. D. Base Release in Nucleosides Induced by Low-Energy Electrons: A Dft Study. *Radiat. Res.* **2006**, *165*, 721−729.

(20) Gu, J.; Wang, J.; Leszczynski, J. Electron Attachment-Induced DNA Single-Strand Breaks at the Pyrimidine Sites. *Nucleic Acids Res.* **2010**, *38*, 5280−5290.

(21) Li, Z.; Zheng, Y.; Cloutier, P.; Sanche, L.; Wagner, J. R. Low Energy Electron Induced DNA Damage: Effects of Terminal Phosphate and Base Moieties on the Distribution of Damage. *J. Am. Chem. Soc.* **2008**, *130*, 5612−5613.

(22) Li, Z.; Cloutier, P.; Sanche, L.; Wagner, J. R. Low-Energy Electron-Induced DNA Damage: Effect of Base Sequence in Oligonucleotide Trimers. *J. Am. Chem. Soc.* **2010**, *132*, 5422−5427.

(23) Becker, D.; Razskazovskii, Y.; Callaghan, M. U.; Sevilla, M. D. Electron Spin Resonance of DNA Irradiated with a Heavy-Ion Beam ($^{16}O^{8+}$): Evidence for Damage to the Deoxyribose Phosphate Backbone. *Radiat. Res.* **1996**, *146*, 361−368.

(24) Becker, D.; Bryant-Friedrich, A.; Trzasko, C.; Sevilla, M. D. Electron Spin Resonance Study of DNA Irradiated with an Argon-Ion Beam: Evidence for Formation of Sugar Phosphate Backbone Radicals. *Radiat. Res.* **2003**, *160*, 174−185.

(25) Zheng, Y.; Cloutier, P.; Hunting, D. J.; Sanche, L.; Wagner, J. R. Chemical Basis of DNA Sugar-Phosphate Cleavage by Low-Energy Electrons. *J. Am. Chem. Soc.* **2005**, *127*, 16592−16598.
(26) Zheng, Y.; Cloutier, P.; Hunting, D. J.; Wagner, J. R.; Sanche, L. Phosphodiester and N-Glycosidic Bond Cleavage in DNA Induced by 4−15 eV Electrons. *J. Chem. Phys.* **2006**, *124*, 064710−064719.
(27) Berdys, J.; Anusiewicz, I.; Skurski, P.; Simons, J. Damage to Model DNA Fragments from Very Low-Energy (<1 eV) Electrons. *J. Am. Chem. Soc.* **2004**, *126*, 6441−6447.
(28) Rak, J.; Kobylecka, M.; Storoniak, P. Single Strand Break in DNA Coupled to the O-P Bond Cleavage. A Computational Study. *J. Phys. Chem. B* **2011**, *115*, 1911−1917.
(29) Ptasinska, S.; Sanche, L. Dissociative Electron Attachment to Hydrated Single DNA Strands. *Phys. Rev. E* **2007**, *75*, 031915.
(30) von Sonntag, C. *The Chemical Basis of Radiation Biology*; Taylor and Francis: London, 1987.
(31) Parr, R. G.; Yang, W. *Density-Functional Theory of Atoms and Molecules*; Oxford University Press: 1989.
(32) Geerlings, P.; De Proft, F.; Langenaeker, W. Conceptual Density Functional Theory. *Chem. Rev.* **2003**, *103*, 1793−1874.
(33) Geerlings, P.; De Proft, F. Conceptual Dft: The Chemical Relevance of Higher Response Functions. *Phys. Chem. Chem. Phys.* **2008**, *10*, 3028−3042.
(34) Parr, R. G.; Yang, W. Density Functional Approach to the Frontier-Electron Theory of Chemical Reactivity. *J. Am. Chem. Soc.* **1984**, *106*, 4049−4050.
(35) Cohen, M. H.; Ganduglia-Pirovano, M. V.; Kudrnovsky, J. Electronic and Nuclear Chemical Reactivity. *J. Chem. Phys.* **1994**, *101*, 8988−8997.
(36) De Proft, F.; Liu, S.; Geerlings, P. Calculation of the Nuclear Fukui Function and New Relations for Nuclear Softness and Hardness Kernels. *J. Chem. Phys.* **1998**, *108*, 7549−7554.
(37) Balawender, R.; Geerlings, P. Nuclear Fukui Function from Coupled Perturbed Hartree-Fock Equations. *J. Chem. Phys.* **2001**, *114*, 682−691.
(38) Balawender, R.; De Proft, F.; Geerlings, P. Nuclear Fukui Function and Berlin's Binding Function: Prediction of the Jahn-Teller Distortion. *J. Chem. Phys.* **2001**, *114*, 4441−4449.
(39) Chamorro, E.; De Proft, F.; Geerlings, P. Generalized Nuclear Fukui Functions in the Framework of Spin-Polarized Density-Functional Theory. *J. Chem. Phys.* **2005**, *123*, 084104−084115.
(40) Insight II biosym/msi accelrys; www.Accelrys.com.
(41) Valiev, M.; Bylaska, E. J.; Govind, N.; Kowalski, K.; Straatsma, T. P.; van Dam, H. J. J.; Wang, D.; Nieplocha, J.; Apra, E.; Windus, T. L.; de Jong, W. A. NWchem: A Comprehensive and Scalable Open-Source Solution for Large Scale Molecular Simulations. *Comput. Phys. Commun.* **2010**, *181*, 1477−1489.
(42) Cornell, W. D.; Cieplak, P.; Bayly, C. I.; Gould, I. R.; Merz, K. M.; Ferguson, D. M.; Spellmeyer, D. C.; Fox, T.; Caldwell, J. W.; Kollman, P. A. A Second Generation Force Field for the Simulation of Proteins, Nucleic Acids, and Organic Molecules. *J. Am. Chem. Soc.* **1995**, *117*, 5179−5197.
(43) Berendsen, H. J. C.; Grigera, J. R.; Straatsma, T. P. The Missing Term in Effective Pair Potentials. *J. Phys. Chem.* **1987**, *91*, 6269−6271.
(44) Darden, T.; York, D.; Pedersen, L. Particle Mesh Ewald: An N-Log(N) Method for Ewald Sums in Large Systems. *J. Chem. Phys.* **1993**, *98*, 10089−10092.
(45) York, D. M.; Darden, T. A.; Pedersen, L. G. The Effect of Long-Range Electrostatic Interactions in Simulations of Macromolecular Crystals: A Comparison of the Ewald and Truncated List Methods. *J. Chem. Phys.* **1993**, *99*, 8345−8348.
(46) Zhao, Y.; Truhlar, D. G. Density Functionals with Broad Applicability in Chemistry. *Acc. Chem. Res.* **2008**, *41*, 157−167.
(47) Zhao, Y.; Truhlar, D. The M06 Suite of Density Functionals for Main Group Thermochemistry, Thermochemical Kinetics, Noncovalent Interactions, Excited States, and Transition Elements: Two New Functionals and Systematic Testing of Four M06-Class Functionals and 12 Other Functionals. *Theor. Chem. Acc.* **2008**, *120*, 215−241.
(48) Johnson, P.; Bartolotti, L.; Ayers, P.; Fievez, T.; Geerlings, P. *Modern Charge-Density Analysis*; Springer: Dordrecht, The Netherlands, 2012; pp 715−764.
(49) Siefermann, K. R.; Abel, B. The Hydrated Electron: A Seemingly Familiar Chemical and Biological Transient. *Angew. Chem., Int. Ed.* **2011**, *50*, 5264−5272.
(50) Seidel, C. A. M.; Schulz, A.; Sauer, M. H. M. Nucleobase-Specific Quenching of Fluorescent Dyes. 1. Nucleobase One-Electron Redox Potentials and Their Correlation with Static and Dynamic Quenching Efficiencies. *J. Phys. Chem.* **1996**, *100*, 5541−5553.
(51) Richardson, N. A.; Gu, J.; Wang, S.; Xie, Y.; Schaefer, H. F. DNA Nucleosides and Their Radical Anions: Molecular Structures and Electron Affinities. *J. Am. Chem. Soc.* **2004**, *126*, 4404−4411.
(52) Das, D.; Eurenius, K. P.; Billings, E. M.; Sherwood, P.; Chatfield, D. C.; Hodoscek, M.; Brooks, B. R. Optimization of Quantum Mechanical Molecular Mechanical Partitioning Schemes: Gaussian Delocalization of Molecular Mechanical Charges and the Double Link Atom Method. *J. Chem. Phys.* **2002**, *117*, 10534−10547.
(53) Senthilkumar, K.; Mujika, J. I.; Ranaghan, K. E.; Manby, F. R.; Mulholland, A. J.; Harvey, J. N. Analysis of Polarization in QM/MM Modelling of Biologically Relevant Hydrogen Bonds. *J. R. Soc., Interface* **2008**, *5*, 207−216.
(54) Gu, J.; Xie, Y.; Schaefer, H. F. Electron Attachment to Nucleotides in Aqueous Solution. *ChemPhysChem* **2006**, *7*, 1885−1887.